EUROPEAN COMMISSION

Community Research

SEVENTH FRAMEWORK PROGRAMME

ARCHER

Collaborative Project (CP)

Co-funded by the European Commission under the Euratom Research and Training Programme on Nuclear Energy within the Seventh Framework Programme

Grant Agreement Number : 269892

Start date : 01/02/2011 Duration : 48 Months

www.archer-project.eu

Archer

Advanced Reactor for Cogeneration of Heat & Electricity-R&D

FEM post-test calculations. Transposition of results to full size IHX – lifetime assessment

Authors : FOKKENS Jan (NRG) , E.J. Sigal (NRG)

ARCHER - Contract Number: 269892
Advanced High-Temperature Reactors for Cogeneration of Heat and Electricity R&D
EC Scientific Officer: Dr. Panagiotis Manolatos

Document title	FEM post-test calculations. Transposition of results to full size IHX – lifetime assessment
Author(s)	FOKKENS Jan , E.J. Sigal (NRG)
Number of pages	39
Document type	Deliverable
Work Package	WP 43
Document number	D43.42
Issued by	NRG
Date of completion	30/01/2015
Dissemination level	Confidential, only for members of the consortium (including the Commission Services).

Summary

This document contains the results from the fatigue evaluations performed for the mock-up of the ARCHER Intermediate Heat Exchanger. The transient thermal data has been calculated by CEA with a CFD calculations. These transient temperatures were used as input for an elastic analysis. With the stress results a linear fatigue and a creep fatigue evaluation has been performed according to the procedures of ASME III-NH. 950°C. For the elastic calculations and the fatigue analyses the general purpose finite element program ANSYS 14.0 was used. Conclusions, recommendations, and implications of results for the full-size mock-up are given.

Approval

Date	By
30/01/2015	Derek BUCKTHORPE
30/01/2015	Derek BUCKTHORPE
30/01/2015	Steven KNOL

Distribution list

Name	Organisation	Comments
P. Manolatos	EC DG RTD	Through the EC participant portal
All beneficiaries	ARCHER	Through the private online workspace

ARCHER IHX
Elastic Fatigue Calculations

Confidential

ARCHER Collaborative Project

Author(s):	E. J. Sigal	reviewed:	J.H. Fokkens
Reference:	NRG-22984/14.129851 Revision 2	approved:	F.J. Blom
37 pages	29 January 2015		

© NRG 2015

Subject to agreement with the client, the information contained in this report may not be disclosed to any third party and NRG is not liable for any damage arising out of the use of such information

Contents

1	Introduction	5
2	Approach and Assumptions	6
3	Model Description	7
3.1	Geometry	7
3.2	Finite Element Model	7
3.3	Boundary Conditions	7
3.4	Loading Conditions	8
4	Material Properties	9
4.1	Young's Modulus	9
4.2	Poison Ratio	10
4.3	Thermal Expansion Coefficient	10
4.4	Allowable Stresses	10
4.5	Fatigue Design Curve	11
5	Fatigue Assessment	12
5.1	Fatigue Analysis	12
5.2	Locations	12
5.3	Fatigue Strength Reduction Factors	12
5.4	Creep Fatigue	12
5.5	Limitations	13
6	Results	14
6.1	Thermo-Mechanical Analysis	14
6.2	Linear Fatigue Assessment	14
6.3	Creep-Fatigue Assessment	14
7	Conclusions	16
8	References	18
9	Figures	19
Appendix A	Results of Fatigue Analysis	34

1 Introduction

This report summarizes the finite element calculations performed for the Intermediate Heat Exchanger (IHX) mock-up within the ARCHER project. Based on the results of the calculations a linear fatigue and a creep fatigue evaluation of the IHX mock-up design have been performed. The fatigue evaluations are performed according to the guidelines in ASME Section III, Division 1 - Subsection NH [5]. The IHX mock-up will be tested by CEA Grenoble in the Claire loop.

In Chapter 2 the followed approach and the assumptions are described.

In Chapter 3 the IHX model is described. For the finite element calculations the same geometric model is used as for the CFD calculations. CEA Grenoble has performed CFD calculations in order to determine the transient thermal behaviour of the IHX mock-up. These transient thermal results are incorporated into the structural finite element calculations as a thermal body load.

Alloy 800H has been selected for the IHX mock-up, and its material properties are summarized in Chapter 4. The elastic material properties used in the FEM model have been taken from [1], [2], [3], [5].

In Chapter 5 the fatigue assessment approach is discussed, and a short description of the main results is given in Chapter 6.

The conclusions and recommendations are presented in Chapter 7, as well as the implications of the results for the full size IHX.

2 Approach and Assumptions

The fatigue behaviour of the IHX mock-up is investigated with elastic finite element calculations. The IHX transient thermal load has been determined with CFD calculations by CEA Grenoble [8]. The thermal transient is comprised of 98 time steps which are used to calculate 98 corresponding stress distributions. The stress distributions represent a complete load cycle for which the fatigue evaluation is performed. The four-plate model used by CEA has been extended to eight plates for the structural analysis with FEM.

3 Model Description

3.1 Geometry

A full IHX mock-up consists of a stack of 16 thin corrugated plates with thick end plates at the top and at the bottom of the stack. The air to the exchanger is supplied and extracted through the bottom plate. CEA [8] modelled the top plate and four corrugated plates (see Figure 1, Figure 2 and Figure 3), taking advantage of the symmetry in the transversal (x) direction of the IHX (see Figure 2). The full length of the mock-up was modelled. Figure 3 shows the solid metal in and around the gas layers and the corrugated section of a single IHX plate.

For the structural finite element model a four-plate geometry presents problems with the boundary conditions at the bottom of the model (the bottom in Figure 2). In order to apply appropriate (in this case symmetry in the z direction) boundary conditions at the bottom of the model, the geometry of the four-plate stack modelled by CEA has been extended to eight plates as shown in Figure 4. The eight-plate model with a symmetry boundary condition gives a reasonable approximation to the structural behaviour of a thermally loaded 16-plate IHX.

3.2 Finite Element Model

Figure 5 shows the finite element mesh used by CEA to model the top four plates of the IHX. Figure 6 shows the mesh for the eight-plate IHX model. The mesh for the top end plate and the first four corrugated plates of the eight-plate model is the same as the mesh for the four-plate model. The mesh for the additional four plates of the eight-plate model was generated from the four-plate mesh by copying the mesh of two bottom plates two times, as depicted in Figure 7.

The eight-plate mesh consists of 302316 elements and 323862 nodes. The finite element calculations have been performed with the general purpose finite element program ANSYS 14.0 [4] using three-dimensional arbitrarily distorted (8 node) brick elements of type SOLID185.

3.3 Boundary Conditions

The boundary conditions for the eight-plate IHX model are shown in Figure 8. Two symmetry boundary conditions are applied, one in the x direction, the other in the z direction. The model is held at a single node to suppress the rigid body motion.

3.4 Loading Conditions

Only thermal loads are applied to the IHX model with the reference (unstrained state) temperature of 293°K. The temperature distributions occurring in the IHX during cool-down and heat-up thermal cycles have been determined with CFD calculations by CEA Grenoble [8]. The cool-down and heat-up cycles combine to form a single thermal transient which is comprised of 98 time steps. For each time step a temperature distribution is applied as a thermal body load in the FEM calculations.

CEA performed CFD calculations for a four-plate model (see Figure 1). However, it is reasonable to assume that for an eight-plate model temperature distributions for plates 3 and 4 can be applied to plates 5 and 6 along with plates 7 and 8. This assumption, which is illustrated in Figure 9, is used for thermal loads of the eight-plate IHX model.

4 Material Properties

The material properties used for the elastic finite element calculations are summarized in the following sections. The material for the IHX is Alloy 800H, and its properties are taken from [1], [2], [3], [5].

4.1 Young's Modulus

Table 1 summarizes the temperature-dependent values of the Young's modulus for Alloy 800H. Figure 10 shows the graphical representation of these data.

Table 1. Alloy 800H – Temperature-dependent Young's modulus.

T [°C]	*T* [°K]	*E* [GPa]
20	293	200
100	373	190
200	473	185
300	573	175
400	673	170
500	773	160
600	873	155
700	973	145
800	1073	140

For the corrugated areas of the plates different Young's moduli are applied in the transversal (x), longitudinal (y), and thickness (z) directions. The applied temperature-dependent Young's moduli are summarized in Table 2 and shown in Figure 11. The Young's moduli for corrugated plates are based on [2].

Table 2. Alloy 800H – Temperature-dependent anisotropic Young's moduli of corrugated plates.

T [°C]	*T* [°K]	E_x [GPa]	E_y [GPa]	E_z [GPa]
20	293	66.8	182.4	200
100	373	63.5	173.3	190
200	473	61.8	168.7	185
300	573	58.4	159.6	175
400	673	56.8	155.0	170
500	773	53.4	145.9	160
600	873	51.8	141.4	155
700	973	48.4	132.2	145
800	1073	46.8	127.7	140

4.2 Poisson Ratio

The Poisson ratio is taken as 0.31 based on Table PRD of [3].

4.3 Thermal Expansion Coefficient

Table 3 summarizes the temperature-dependent values of the mean thermal expansion coefficient for Alloy 800H, [1]. Figure 12 shows the graphical presentation of the data for the coefficient of thermal expansion.

Table 3. Alloy 800H – Temperature-dependent mean (α_m) thermal expansion coefficients.

T [°C]	T [°K]	α_m [10^{-6} K^{-1}]
20	293	15.0
100	373	15.4
200	473	16.0
300	573	16.5
400	673	16.8
500	773	17.2
600	873	17.5
700	973	17.9
800	1073	18.3

4.4 Allowable Stresses

The values of allowable stresses S_m for Alloy 800H are shown in Table 4 and Figure 13. The values of S_m are based on Figure I-14.3C of ASME III-NH [5], which is reproduced in Figure 14 for a reference. The S_m data in Table 4 have been obtained by digitizing the curve in Figure 14 and linearly extrapolating the S_m values below 426.7 °C and above 760 °C.

Table 4. Allowable stresses S_m for Alloy 800H.

T [°C]	S_m [MPa]
100	123.8
537	99.6
649	95.4
666	94.7
678	93.8
691	92.7
706	90.8
719	88.3
730	85.8
741	82.9
900	34.4

4.5 Fatigue Design Curve

Fatigue design curves for Alloy 800H at 800°C are given in Table 5 and plotted in Figure 15 and Figure 16, [1]. Table 5 shows both strain and stress S_a as functions of allowable number of cycles. Only strain fatigue curves were available in [1], but the stress design curves are required for fatigue analysis in ANSYS. Consequently, the 800°C strain curve has been digitized, and the strain values have been multiplied by the Young's modulus of 140 GPa (modulus at 800 °C) to give the values for S_a.

Table 5. Fatigue design curves for Alloy 800H at 800 °C.

Number of Cycles	Strain [%]	S_a [MPa]
4.9	3.44	4,822.1
9.7	2.22	3,110.2
19.1	1.46	2,047.7
30.4	1.08	1,509.1
53.8	0.80	1,123.8
93.9	0.61	849.9
161.9	0.48	673.2
288.3	0.38	526.4
913.7	0.27	372.7
2,941.0	0.20	274.2
9,215.2	0.15	212.4
27,511.0	0.13	176.3

5 Fatigue Assessment

Fatigue assessment of the IHX mock-up was performed according to ASME Section III, Division 1, Subsection NH [5]. This approach is chosen for the IHX mock-up, because a full size IHX has to be evaluated according to a commercial code such as ASME III. However, utilizing a commercial code will result in conservative results for the fatigue evaluation. In this chapter, various aspects of fatigue analysis are described.

5.1 Fatigue Analysis

Fatigue analysis was performed using the POST1 postprocessor of ANSYS, version 14.0, [4], for a single transient load case which was provided by CAE with the CFD simulation [8].

5.2 Locations

The focus areas for fatigue evaluation are located at the interface of the corrugated plates and the air-inlet and air-outlet channels, i.e. the edges of the circular openings in the corrugated plates. The hot side of IHX is more at risk because allowable stresses are lower due to higher temperature levels. Consequently, for each circular opening four locations (at the angles of 0, 90, 180 and 270 degrees) have been selected for fatigue evaluation. On the cold side, the same angle locations have been selected, but only for the top two corrugated plates. In addition, two areas of high stresses at the circular openings have been chosen for fatigue evaluation. The locations of fatigue evaluations, along with the corresponding linearization paths, are shown in Figure 17 and Figure 18. In total, fatigue was evaluated at 146 locations.

5.3 Fatigue Strength Reduction Factors

In accordance with ASME 2010, Table NB-3681(a)-1,[7] a fatigue strength reduction factor of 1.8 (most conservative for as-is welds) should be applied at the locations of the welds. The factor of 1.8 is used in the current analysis.

5.4 Creep Fatigue

The creep fatigue evaluation is performed according to the procedures described in Appendix T of ASME Section III, Division 1 - Subsection NH (Article T-1400). The creep-fatigue damage at the end of the design life has to fulfil the following relation,

$$\sum_{j=1}^{p}\left(\frac{n}{N_d}\right)_j + \sum_{k=1}^{q}\left(\frac{\Delta t}{T_d}\right)_k \leq D$$

The damage limit D in the above equation is taken from Figure T-1420-2 in Appendix T. The fatigue damage is determined according to the procedure described in article T-1432. The number of allowable

fatigue cycles N_d is determined with the design fatigue strain ranges given in Figure T-1420-1C and linearly interpolated and extrapolated to appropriate operational temperatures. The fatigue strain range is calculated according to T-1432(h),

$$\Delta\epsilon_t = K_\nu \cdot \Delta\epsilon_{\text{mod}} + K \cdot \Delta\epsilon_c$$

5.5 Limitations

Fatigue evaluation method based on the ASME standard, which is implemented in ANSYS, is applicable for temperatures up to 425°C (Table XIII-1153(a)-1, [6]). The operating temperature of the IHX exceeds this limit; consequently, creep-fatigue rather than linear fatigue is the appropriate method for fatigue evaluation. However, the linear fatigue analysis can serve as an initial guide for assessing potential failures due to fatigue.

6 Results

6.1 Thermo-Mechanical Analysis

The results of finite element analysis for the model described in Chapter 3 are summarized in Table 6. The table lists stress intensities at three locations with the largest magnitudes of stress intensities in the area of interest (i.e. the interfaces of the secondary outlet channel). The geometrical locations and the stress intensity contours are shown in Figure 19. Figure 20 shows IHX geometry details in order to enable easier visualisation of stress locations shown in Figure 19. The temperature and stress intensity transients for all three locations are given in Figure 21 and Figure 22 respectively.

6.2 Linear Fatigue Assessment

Table 6 summarizes the values of allowable fatigue cycles at the three locations of high stress based on the simplified elastic (linear) analysis. It can be seen from Figure 22 that all three stress intensity curves have similar magnitudes in the first set of peaks (at the end of the cool-down period). However, in the second set of peaks (at the end of the heat-up period) the `P2_top_300deg` curve has significantly larger magnitude than the other two curves. Consequently, the stress intensity range at this locations is the largest which leads to the lowest number of allowable cycles.

Table 6. Results for linear fatigue evaluation for locations with three lowest values of allowable number of cycles.

Label	Location Description	Maximum Stress Intensity [MPa]	Number of Allowable Cycles
`P2_top_300deg`	2nd corrugated plate, top surface, edge of circular opening at 300°	267	106
`P3_bot_152deg`	3rd corrugated plate, bottom surface, edge of circular opening at 152°	260	168
`P4_top_152deg`	4th corrugated plate, top surface, edge of circular opening at 152°	263	135

6.3 Creep-Fatigue Assessment

Creep-fatigue assessment has been performed for location `P2_top_300deg` because it has the lowest number of allowable cycles based on the linear fatigue analysis. As expected, inclusion of creep into the fatigue analysis further reduces the number of allowable cycles from 106 to 35 as summarized in Table 7.

Table 7. Results for creep-fatigue evaluation for the location with lowest value of allowable number of cycles.

Label	Location Description	Maximum Stress Intensity [MPa]	Number of Allowable Cycles
P2_top_300deg	2nd corrugated plate, top surface, edge of circular opening at 300°	267	35

7 Conclusions and Recommendations

7.1 Conclusions

In this report, fatigue assessments of the IHX mock-up are presented. The assessments were performed according to ASME Section III, Division 1 - Subsection NH [5] based on the thermal loading provided by CEA Grenoble [8]. The areas of interest for fatigue evaluation are located at the interfaces to the secondary outlet channel, particularly on the hot side of the IHX.

Both the linear fatigue and creep-fatigue assessments confirmed that the IHX mock-up is vulnerable to fatigue failure at the interfaces to the secondary outlet channel in the top part of the IHX on its hot side before reaching the desired 1000 operational cycles. The difference in stiffness between the active (corrugated) plates and the thick end plates results in high stress levels. The linear fatigue analysis predicted 106 allowable cycles while the creep-fatigue analysis predicted 35 allowable cycles. Fatigue analyses according to the ASME III code are conservative. Results of linear fatigue analysis should be viewed with caution and used only as a guideline due to the assumption of elastic strain and stress.

7.2 Recommendations

The elastic finite element calculations have been performed with the same mesh as the CFD calculations. For the CFD calculations the modelling was sufficient. For the mechanical calculations no correct symmetry boundary condition could be applied on the four plate model, which influenced the stress behaviour unfavourably. Expanding the model to an eight plate model, so that a real symmetry boundary conditions could be applied, resulted in a better prediction of the stress behaviour. However, the model was too coarse near the interfaces to the secondary outlet channel in the top for the mechanical calculations. Phenomena such as bending were not modelled correctly. Stress levels at geometric discontinuities were exaggerated, which makes the results of the fatigue assessments more conservative. The finite element mesh should be optimized for mechanical calculations around the geometric discontinuities in the plates at the secondary outlet channel.

The difference in stiffness between the top active (corrugated) plates and the end plates should be reduced. This results in a reduction of the stress levels in the active plates next to the end plates.

A fatigue evaluation based on the stress levels calculated with a non-linear (creep) calculation will give better, less conservative results.

7.3 Implications for full size IHX

The full size IHX, to be installed in a HTR, will be manufactured of the same plate geometry and material as the mock-up. The full-size IHX has more active plates and a different process medium (He-He instead of air-air) will be used. For the full-size IHX the highly stressed locations (near the interfaces to the secondary outlet channel in the active plates next to the end plates) will not change. However, due to the He-He thermal cycle the stress/strain cycles will be different and thus the fatigue results.

Extrapolating the fatigue results of the mock-up to the full-size IHX should not be done. The non-linear behaviour of fatigue makes the results of such an extrapolation to be viewed with care.

Better results would be obtained if a fatigue evaluation is performed based on the stress/strain cycles calculated with the 8-plate mock-up model loaded by the transient temperatures of the He-He thermal cycle.

8 References

[1] D. Buckthorpe. *Review of existing data on Alloy 800H (focusing on thin sheet) and produce results applicable to mock-up and IHX*. ARCHER Deliverable D-43.51, 31 August 2011.

[2] F. Baurand. *ARCHER PROGRAM - Equivalent stiffness of corrugated plate.* PACKINOX note Revision B, 1 February 2012.

[3] *ASME Boiler & Pressure Vessel Code - An International Code, Section II, Part D (Customary), Materials.* The American Society of Mechanical Engineers, 2010 Edition, 1 July 2010.

[4] *ANSYS User Manuals Release 14.0*. ANSYS Inc.

[5] *ASME Boiler & Pressure Vessel Code - An International Code, Section III, Division 1 – Subsection NH*, The American Society of Mechanical Engineers, 2011a Edition, July 2011

[6] *ASME Boiler & Pressure Vessel Code - An International Code, Section III, Division 1 – Appendices.* The American Society of Mechanical Engineers, 2010 Edition, 1 July 2010.

[7] *ASME Boiler & Pressure Vessel Code - An International Code, Section III, Division 1 – Subsection NB.* The American Society of Mechanical Engineers, 2010 Edition, 1 July 2010

[8] P. Bonnamy. Personal E-mail message 20121213 18:38, 13 December 2012

9 Figures

This page is intentionally left blank.

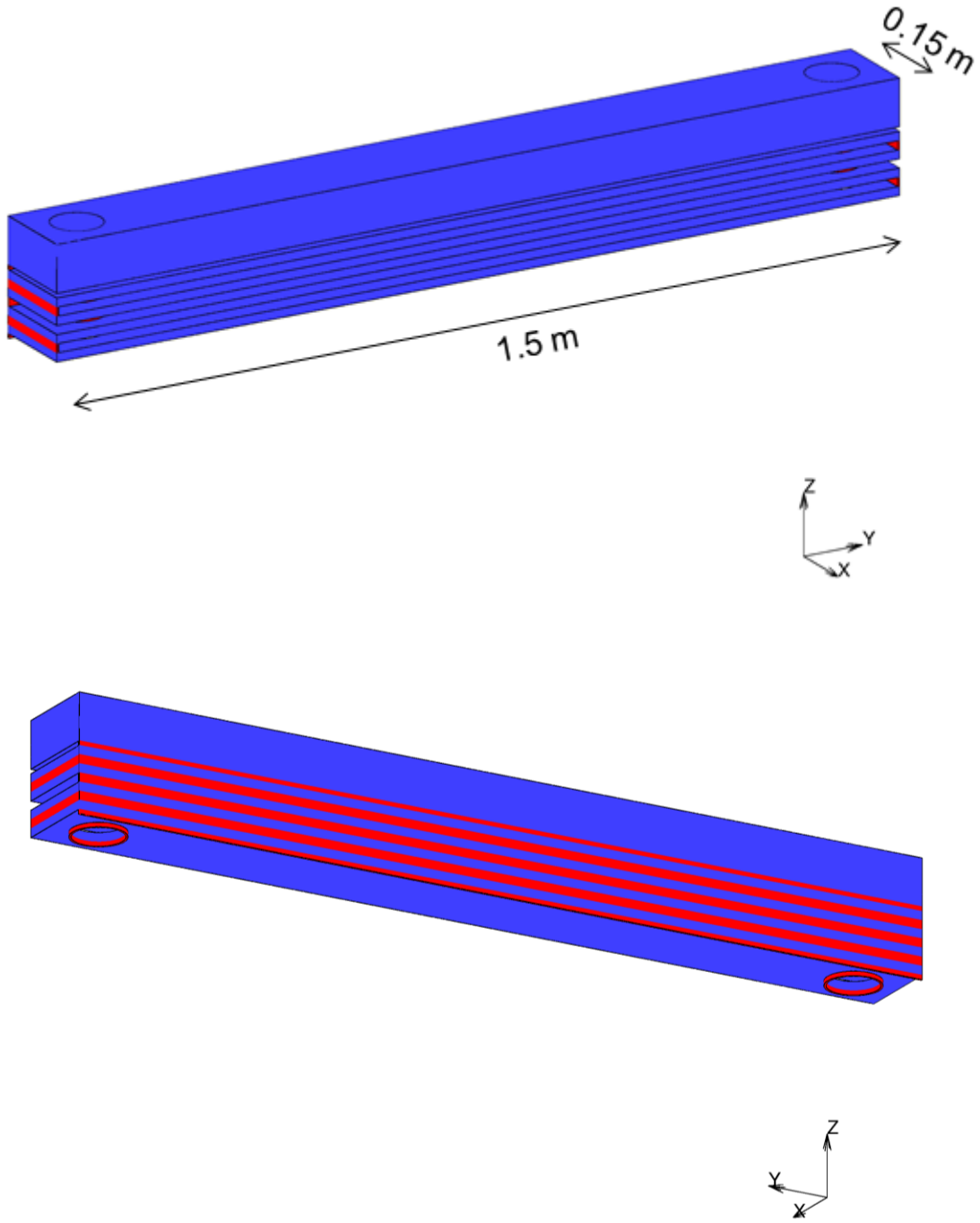

Figure 1. Four-plate model of the Intermediate Heat Exchanger. Geometry scaled by a factor of 10 in the *z* direction.

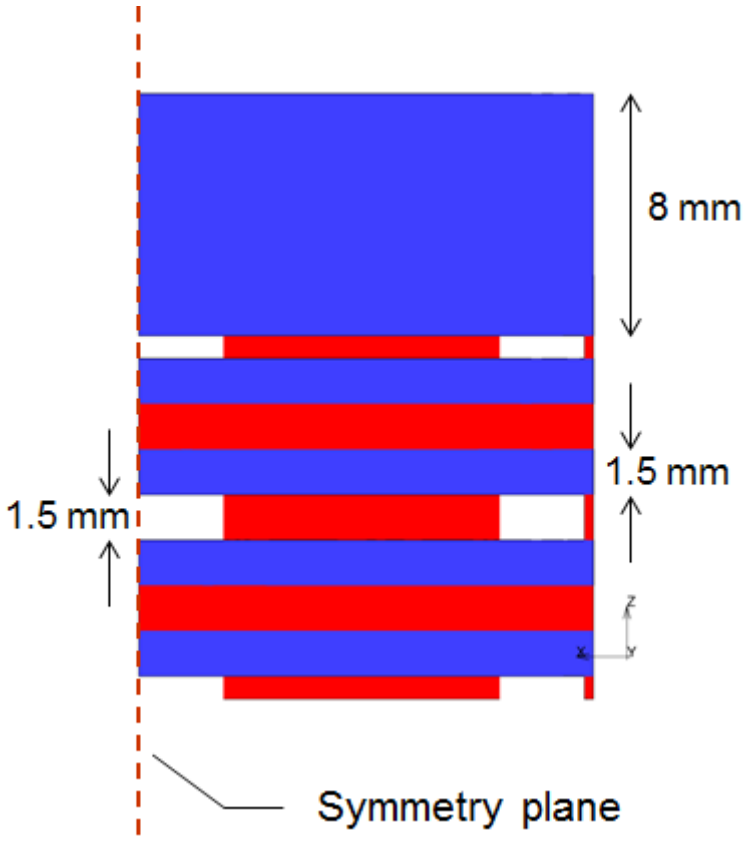

Figure 2. Four-plate model of the Intermediate Heat Exchanger. Geometry scaled by a factor of 10 in the *z* direction.

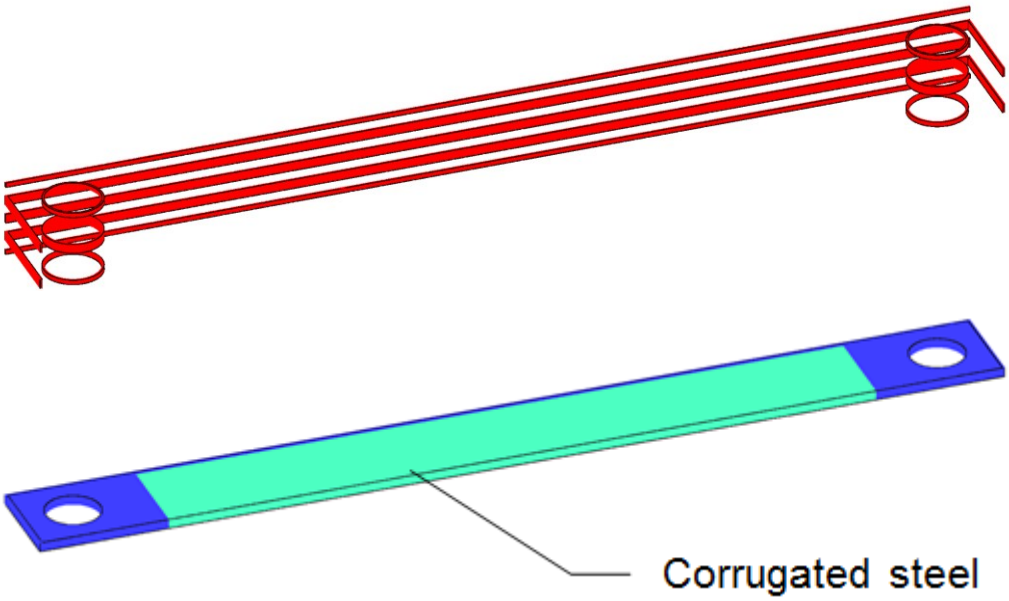

Figure 3. Details of four-plate IHX model. Geometry scaled by a factor of 10 in the *z* direction.

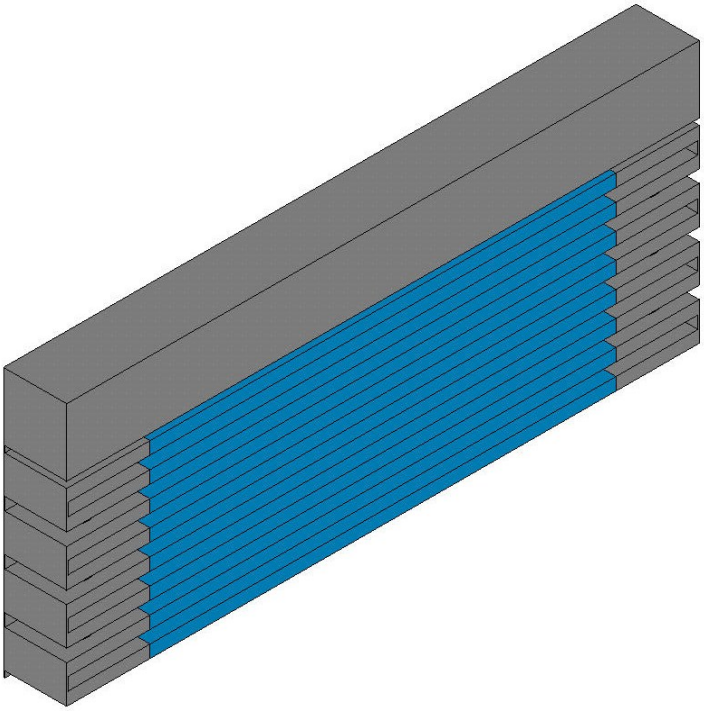

Figure 4. Eight-plate model of the Intermediate Heat Exchanger. Geometry scaled by a factor of 20 in the *z* direction.

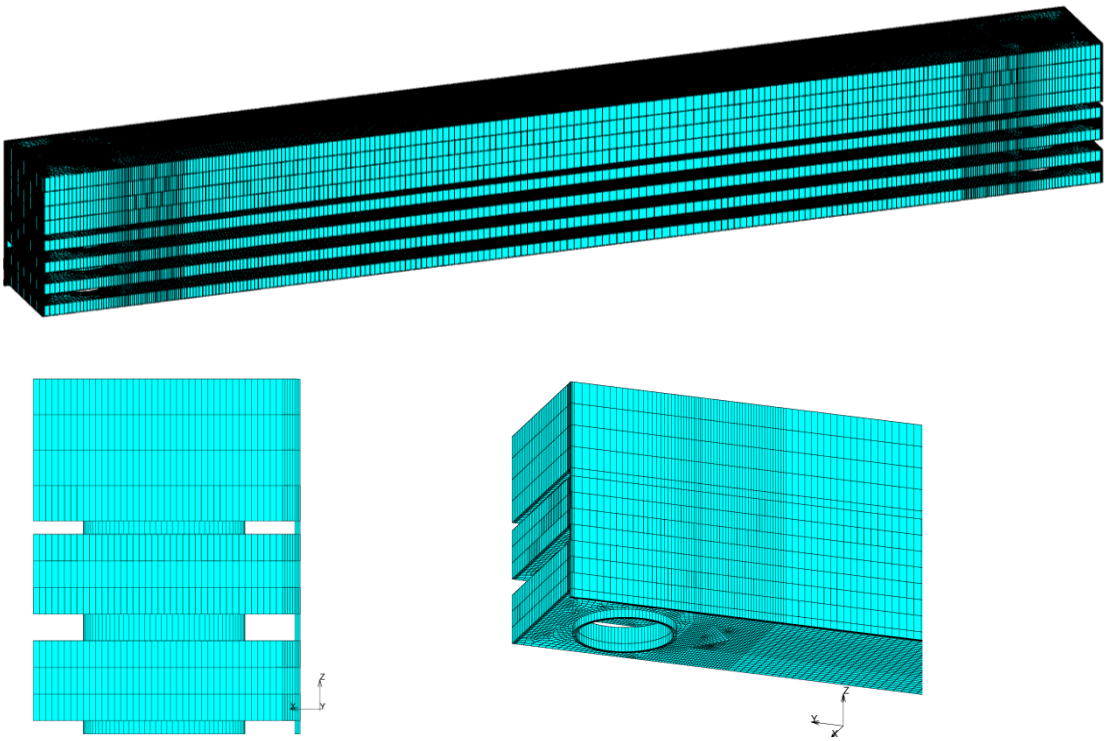

Figure 5. Mesh for the four-plate IHX model (from CEA CFD calculations). Geometry scaled by a factor of 10 in the *z* direction.

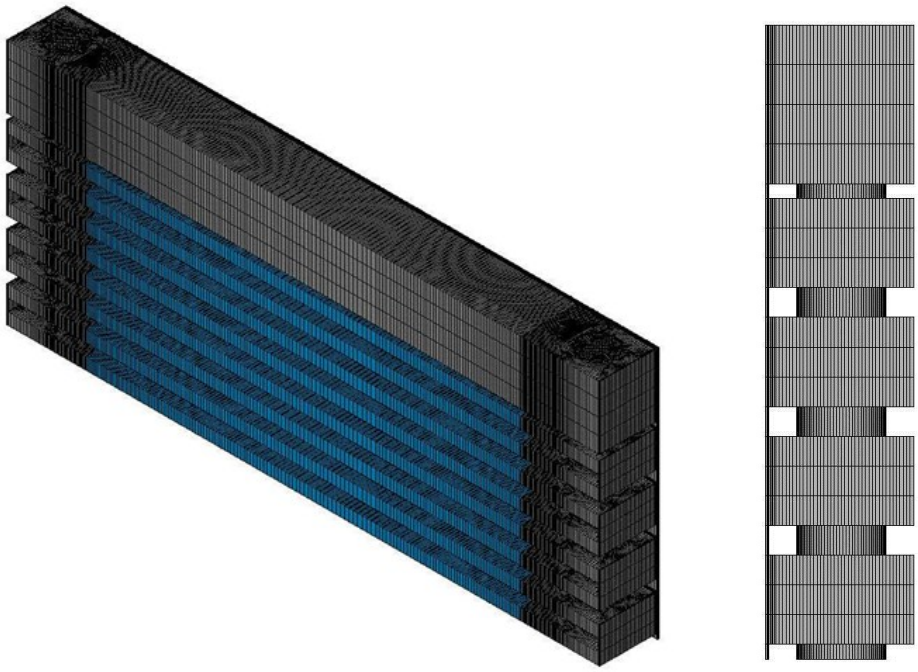

Figure 6. Mesh for the eight-plate IHX model. Geometry scaled by a factor of 20 in the *z* direction.

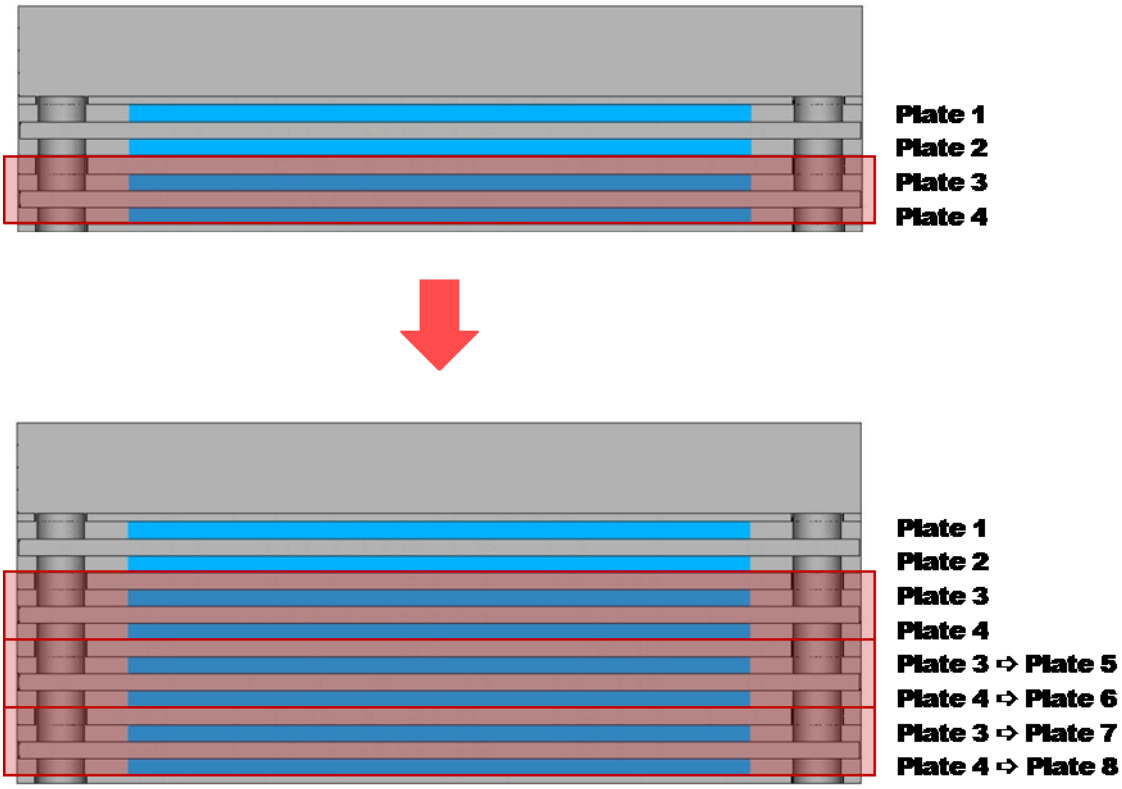

Figure 7. A four-plate model extended to an eight-plate by copying Plate 3 and Plate 4 two times. Geometry scaled by a factor of 20 in the *z* direction.

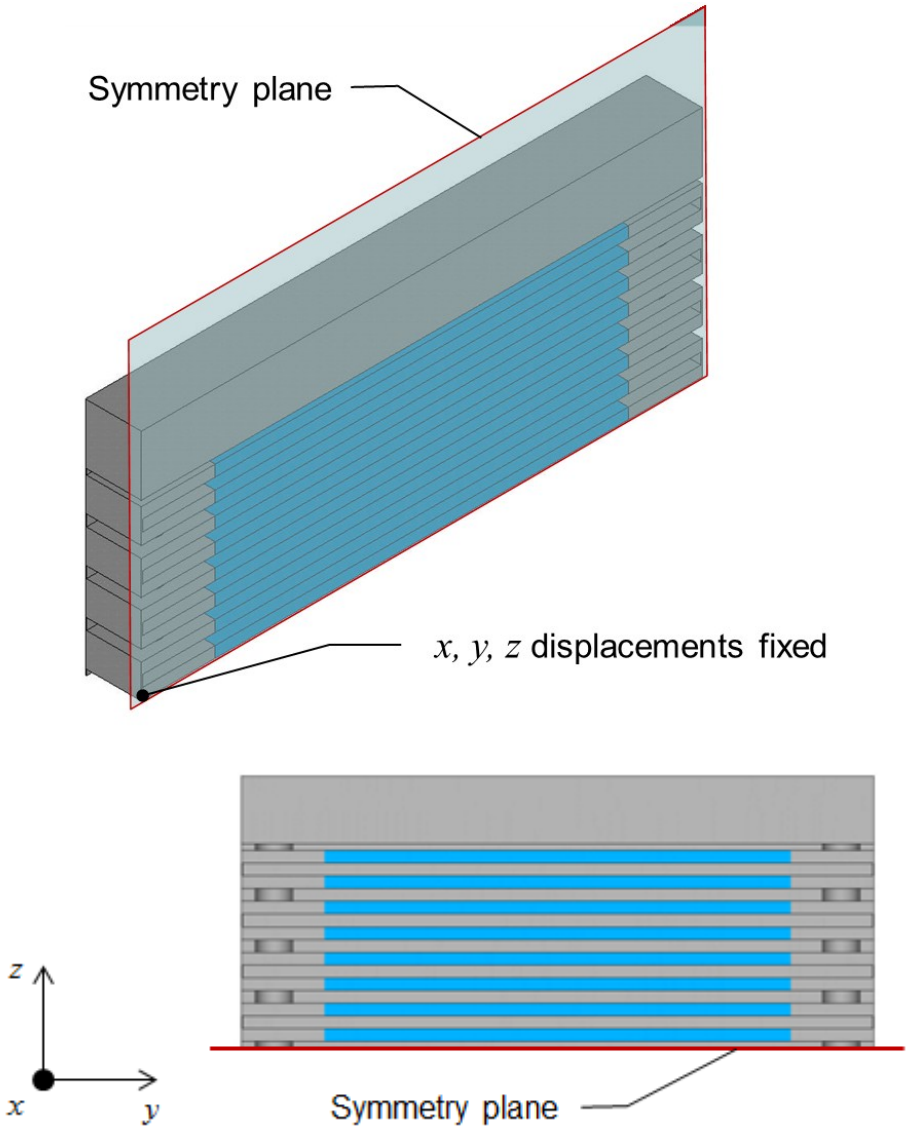

Figure 8. Boundary conditions for the eight-plate IHX model. Geometry scaled by a factor of 20 in the *z* direction.

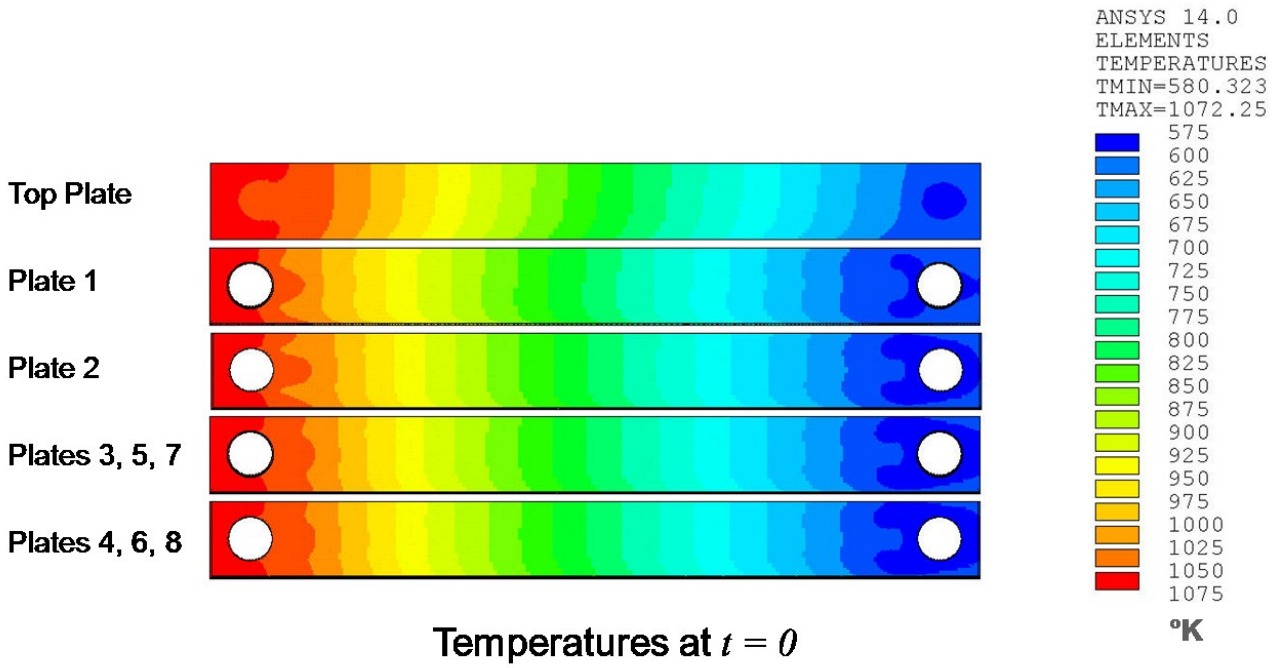

Figure 9. Temperature distribution of the four-plate IHX model as calculated by CEA using a CFD model at time zero. The temperature distribution for Plate 3 is applied to Plate 5 and Plate 7 of the eight-plate structural model. The temperature distribution for Plate 4 is applied to Plate 6 and Plate 8 of the eight-plate structural model.

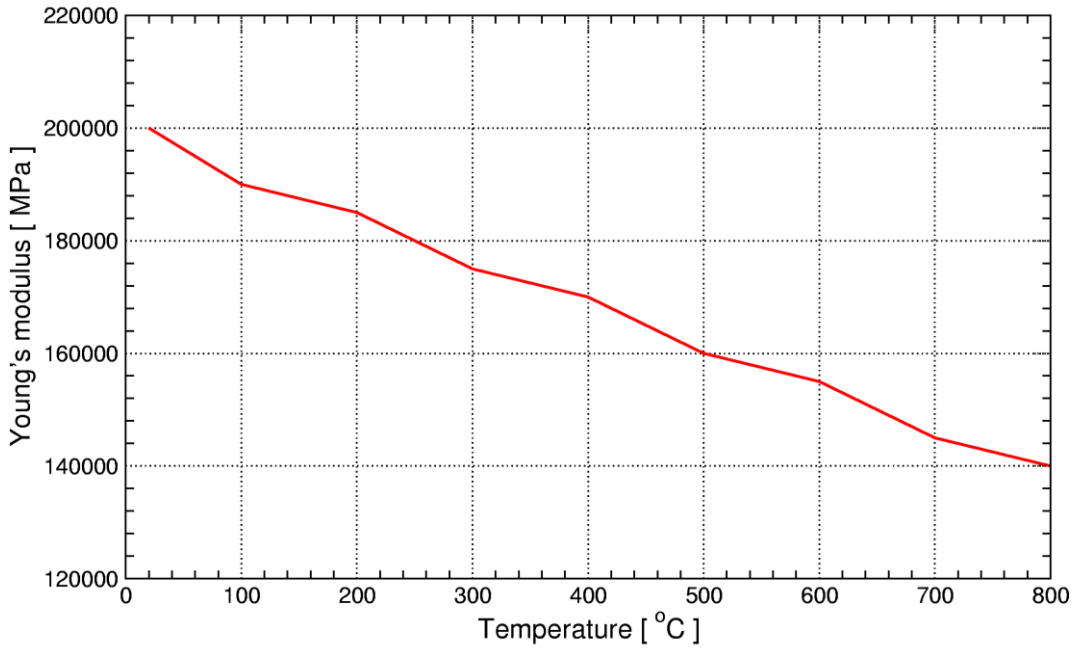

Figure 10. Young's modulus for Alloy 800H as a function of temperature.

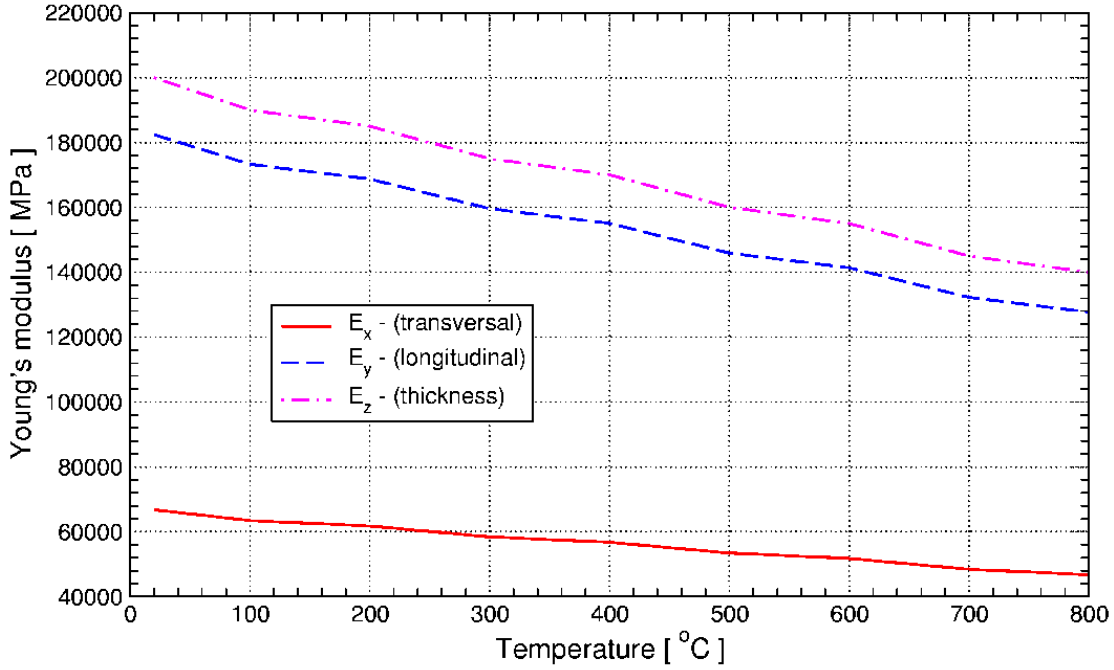

Figure 11. Anisotropic Young's moduli for corrugated portions of Alloy 800H plates as a function of temperature.

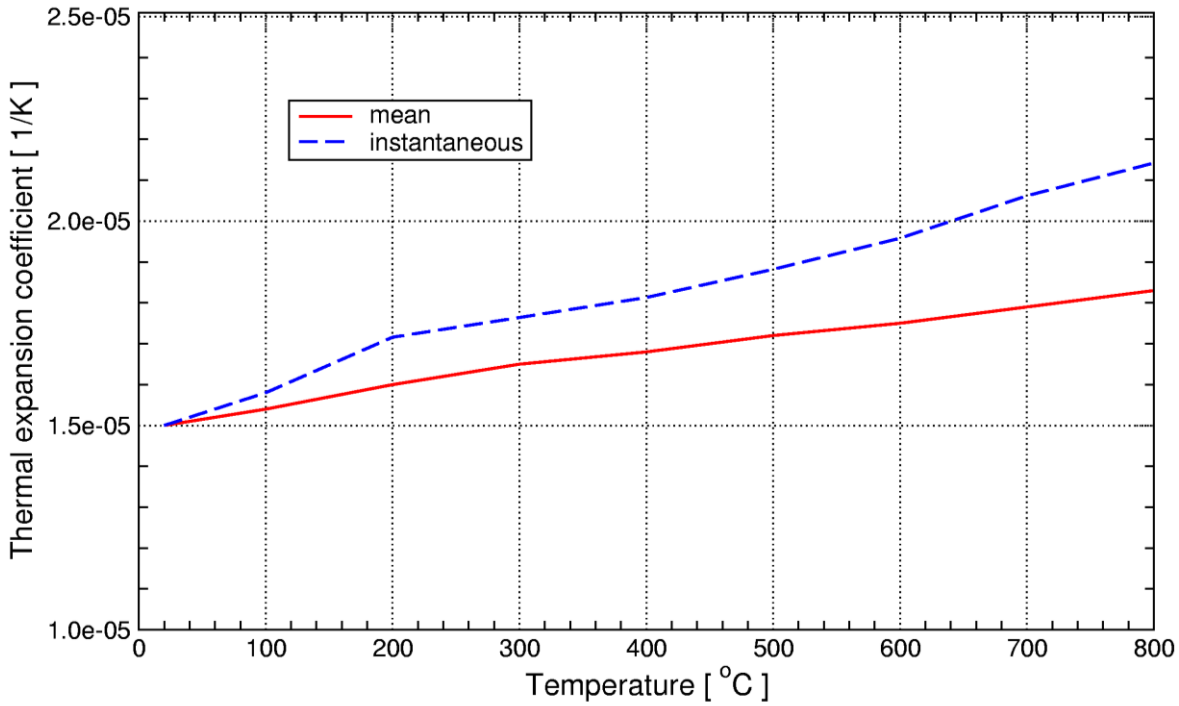

Figure 12. Thermal expansion coefficient for Alloy 800H as a function of temperature.

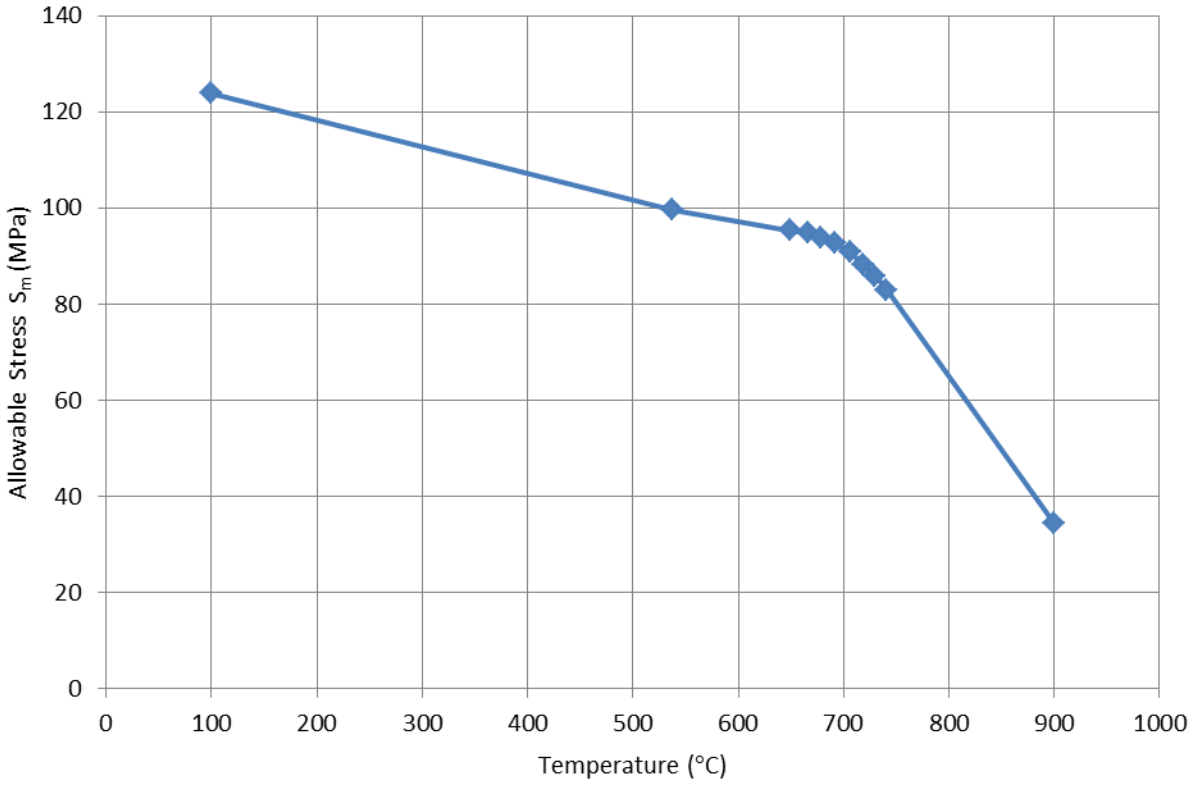

Figure 13. Allowable stress S_m for Alloy 800H as a function of temperature.

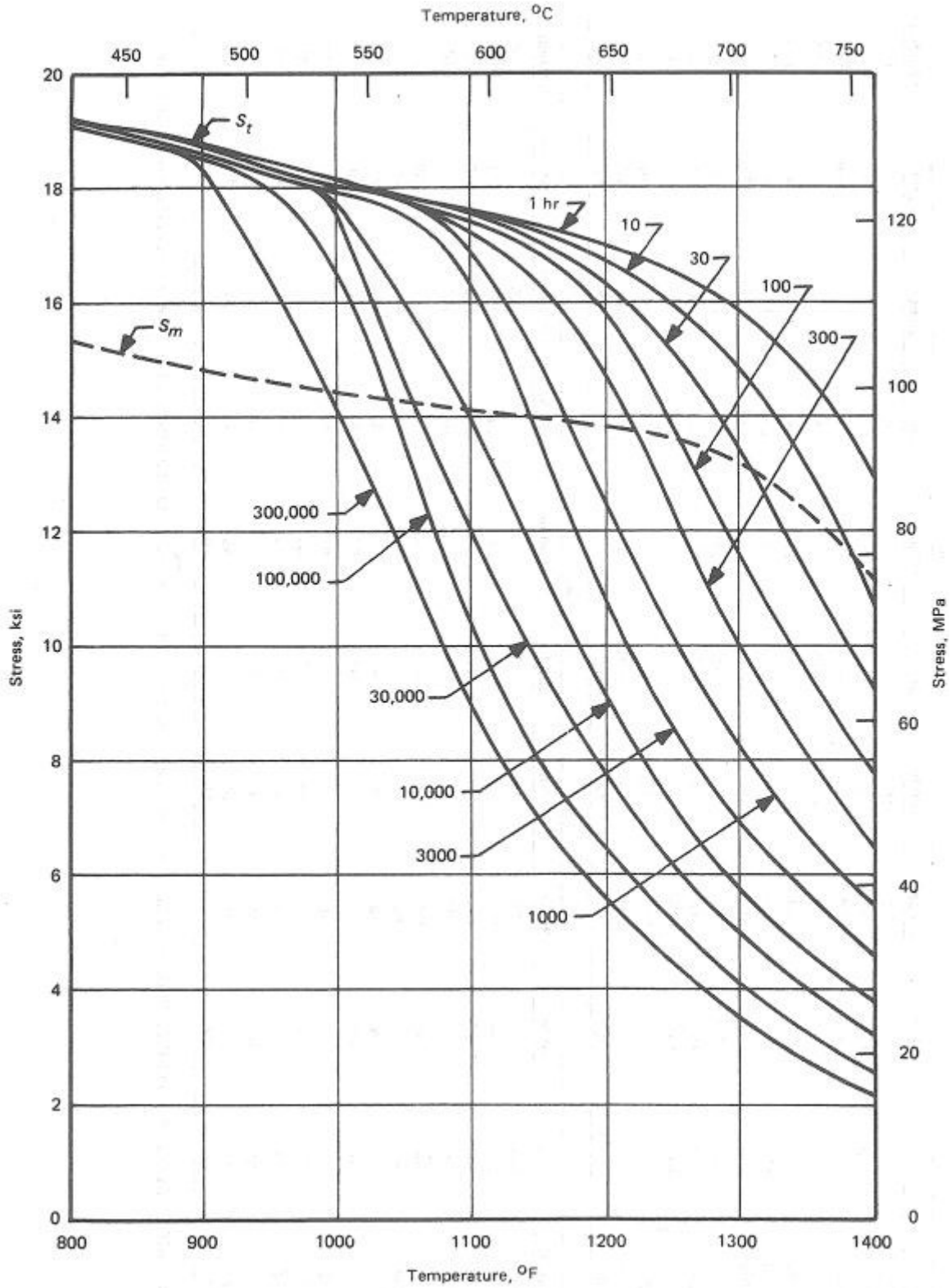

Figure 14. Allowable stress S_m for Alloy 800H as a function of temperature from Figure I-14.3C, [5].

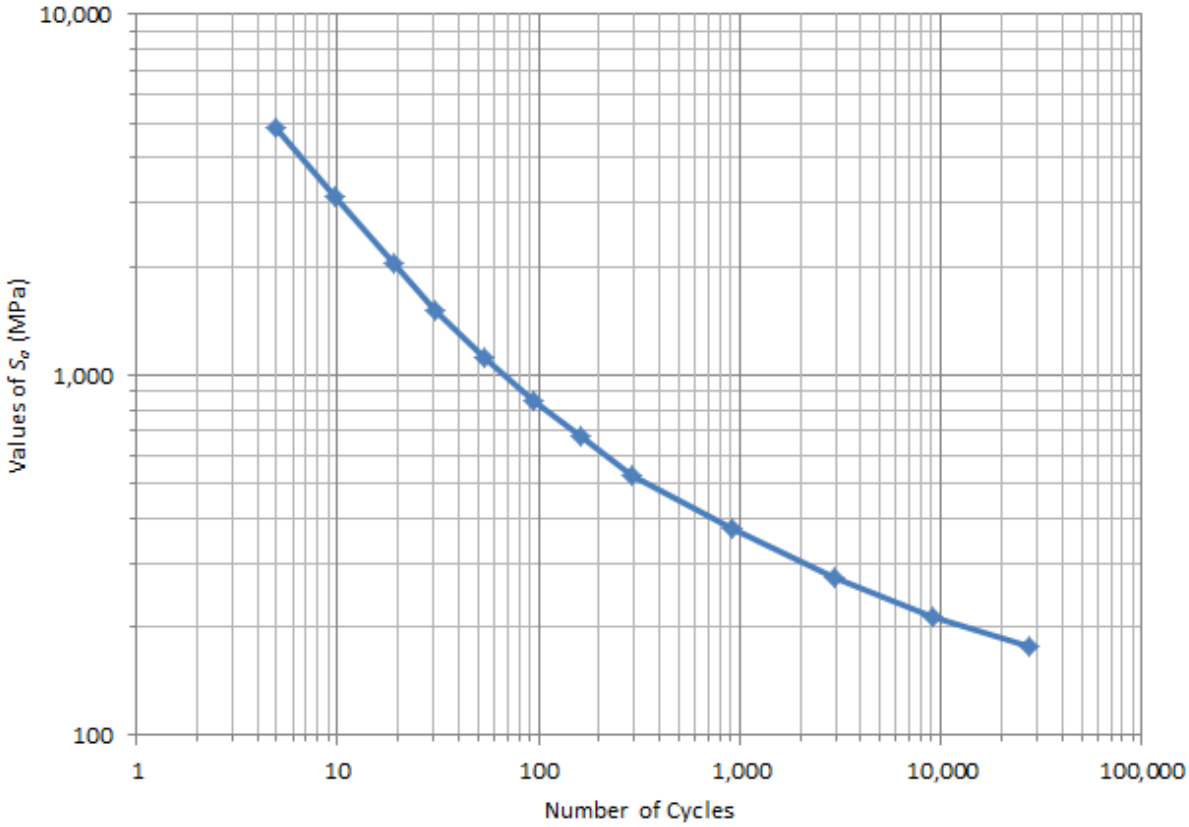

Figure 15. Calculated stress fatigue design curve for Alloy 800H based on strain design curve from [1].

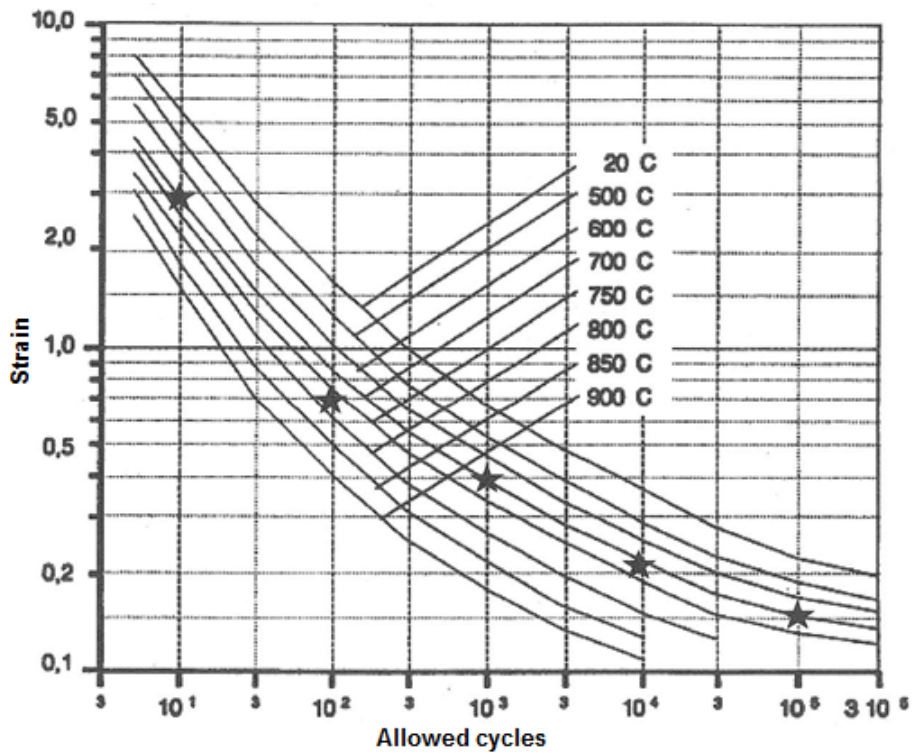

Figure 16. Strain fatigue design curve for Alloy 800H, [1].

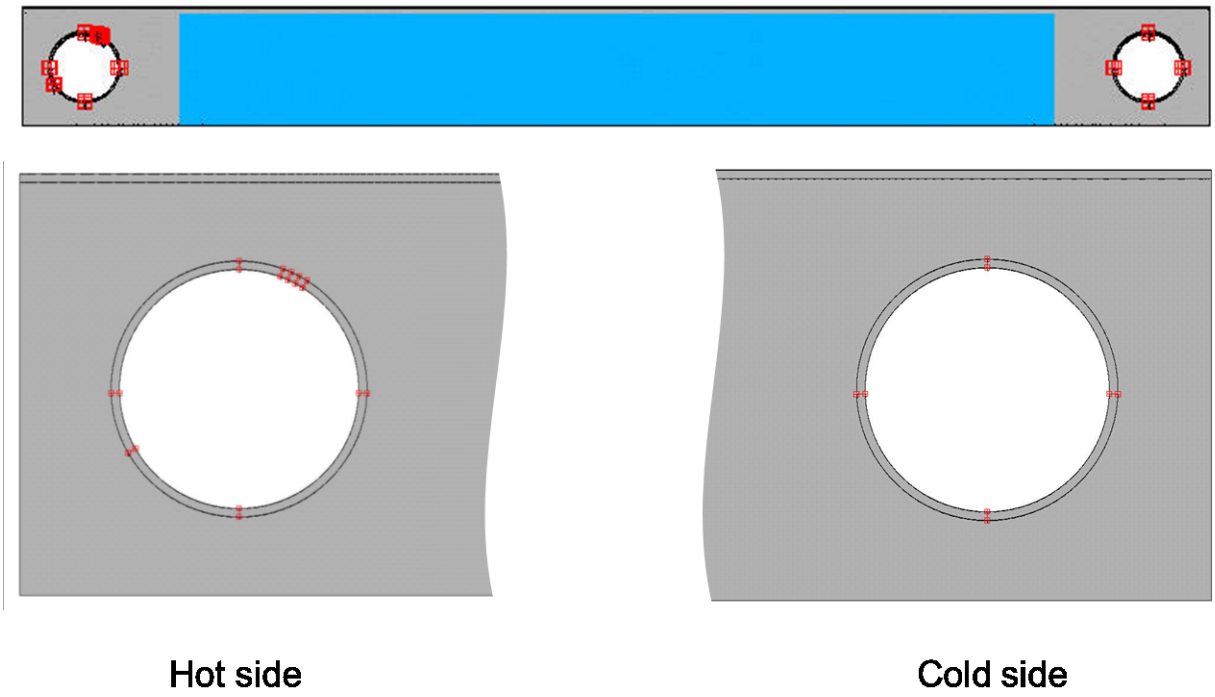

Figure 17. Locations for fatigue evaluation, top view of the IHX.

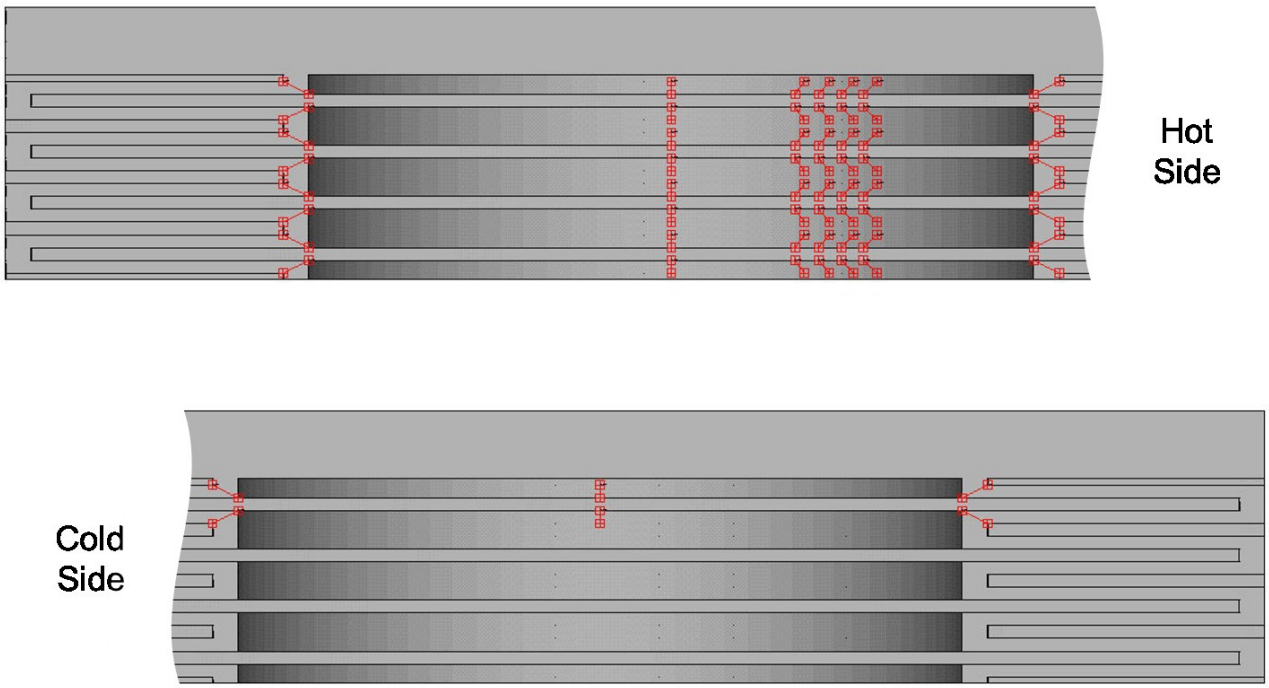

Figure 18. Linearization paths for fatigue evaluation, side view of the IHX. Geometry scaled by a factor of 20 in the *z* direction

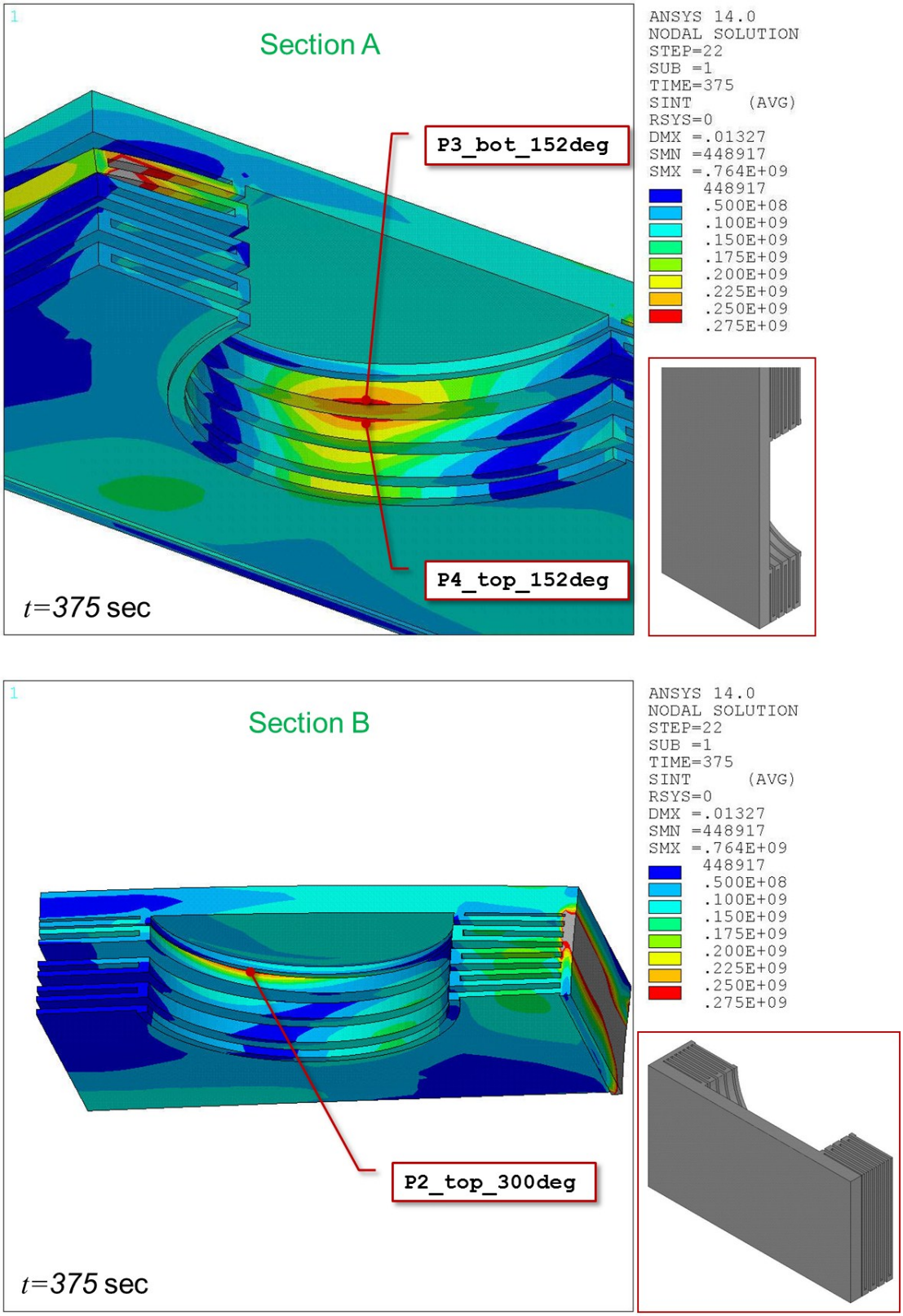

Figure 19. Cross sections of the hot side of the IHX showing locations of high stress intensities at the time of 375 seconds. Reference views of model sections A and B are shown in Figure 20.

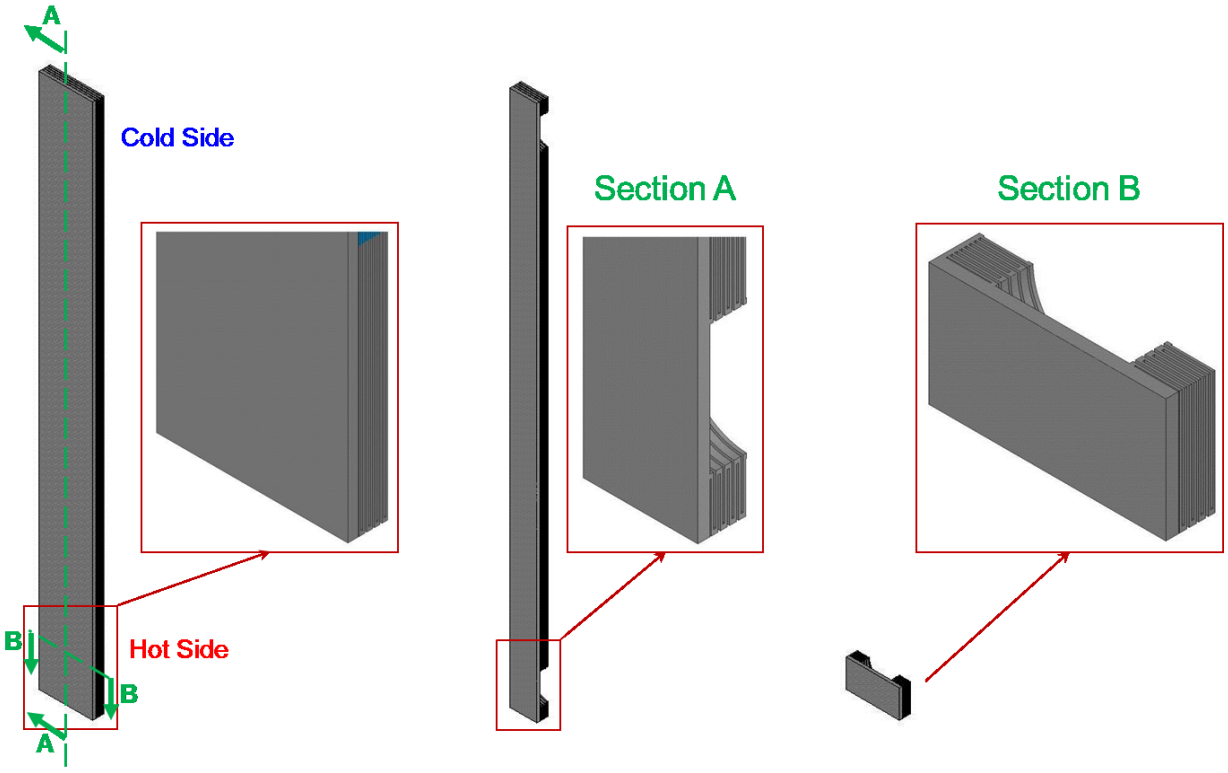

Figure 20. Cross section views of the IHX. Sections A and B are used in Figure 19 to display stress intensities.

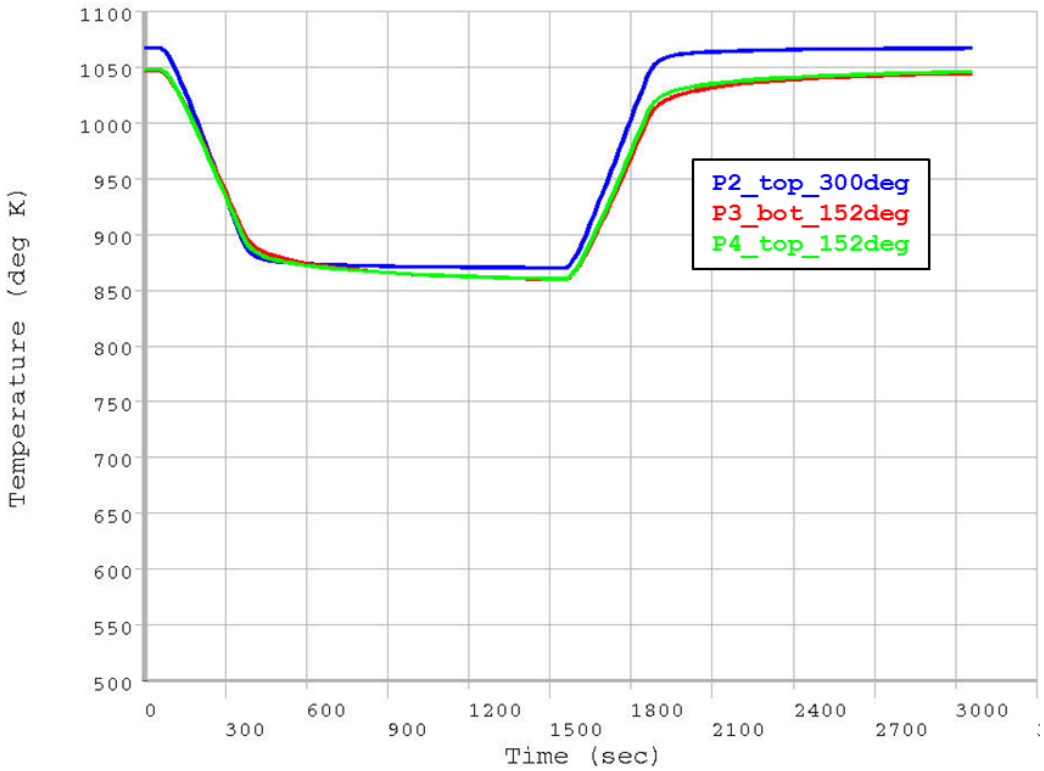

Figure 21. IHX temperature transients for locations shown in Figure 19.

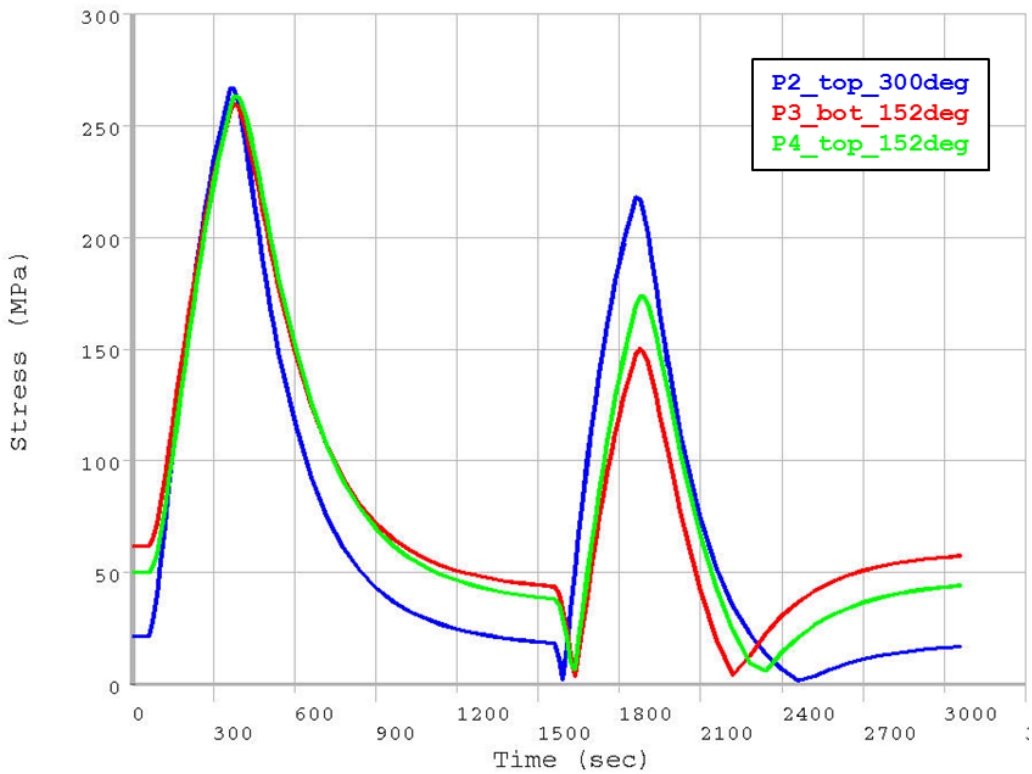

Figure 22. IHX stress intensity transients for locations shown in Figure 19.

Appendix A Results of Fatigue Analysis

Table 8. Results for ANSYS fatigue evaluation for all 146 locations.

Label	S_{alt} [Pa]	T [°K]	Number of Allowable Cycles
hside_p2_bot_300deg	0.24231E+09	1042.3	105.8
hside_p2_top_300deg	0.16864E+09	1043.6	1079.
hside_p8_bot_0deg	0.27931E+08	1046.5	≥ 0.3E+5
hside_p8_top_0deg	0.24493E+08	1046.0	≥ 0.3E+5
hside_p8_bot_90deg	0.88384E+08	1012.4	≥ 0.3E+5
hside_p8_top_90deg	0.11502E+09	1011.5	≥ 0.3E+5
hside_p8_bot_180deg	0.10078E+09	1035.8	≥ 0.3E+5
hside_p8_top_180deg	0.10438E+09	1037.6	≥ 0.3E+5
hside_p8_bot_270deg	0.79064E+08	1051.9	≥ 0.3E+5
hside_p8_top_270deg	0.60389E+08	1050.7	≥ 0.3E+5
hside_p8_bot_148deg	0.13830E+09	1019.5	≥ 0.3E+5
hside_p8_top_148deg	0.15988E+09	1017.3	1952.
hside_p8_bot_152deg	0.14416E+09	1022.2	0.1190E+05
hside_p8_top_152deg	0.16795E+09	1019.8	1081.
hside_p8_bot_156deg	0.14781E+09	1025.0	7682.
hside_p8_top_156deg	0.17252E+09	1022.6	801.6
hside_p8_bot_160deg	0.14705E+09	1023.8	7855.
hside_p8_top_160deg	0.17295E+09	1025.3	787.3
hside_p7_bot_0deg	0.13453E+08	1026.6	≥ 0.3E+5
hside_p7_top_0deg	0.12156E+08	1044.3	≥ 0.3E+5
hside_p7_bot_90deg	0.13851E+09	1010.9	≥ 0.3E+5
hside_p7_top_90deg	0.10773E+09	1004.8	≥ 0.3E+5
hside_p7_bot_180deg	0.85272E+08	1030.3	≥ 0.3E+5
hside_p7_top_180deg	0.84475E+08	1032.9	≥ 0.3E+5
hside_p7_bot_270deg	0.66190E+08	1047.1	≥ 0.3E+5
hside_p7_top_270deg	0.83263E+08	1048.7	≥ 0.3E+5
hside_p7_bot_148deg	0.12923E+09	1014.2	≥ 0.3E+5
hside_p7_top_148deg	0.11805E+09	1014.0	≥ 0.3E+5
hside_p7_bot_152deg	0.13918E+09	1013.9	0.1959E+05
hside_p7_top_152deg	0.12487E+09	1012.9	≥ 0.3E+5
hside_p7_bot_156deg	0.14506E+09	1017.0	8165.
hside_p7_top_156deg	0.12941E+09	1016.1	≥ 0.3E+5
hside_p7_bot_160deg	0.14680E+09	1020.2	6830.
hside_p7_top_160deg	0.12887E+09	1019.3	≥ 0.3E+5
hside_p6_bot_0deg	0.22269E+08	1046.3	≥ 0.3E+5
hside_p6_top_0deg	0.31640E+08	1046.0	≥ 0.3E+5
hside_p6_bot_90deg	0.85018E+08	1009.5	≥ 0.3E+5
hside_p6_top_90deg	0.98241E+08	1015.7	≥ 0.3E+5
hside_p6_bot_180deg	0.93910E+08	1034.6	≥ 0.3E+5

hside_p6_top_180deg	0.10858E+09	1033.6	≥ 0.3E+5
hside_p6_bot_270deg	0.65524E+08	1043.3	≥ 0.3E+5
hside_p6_top_270deg	0.35663E+08	1059.5	≥ 0.3E+5
hside_p6_bot_148deg	0.13420E+09	1017.2	≥ 0.3E+5
hside_p6_top_148deg	0.18226E+09	1017.3	487.2
hside_p6_bot_152deg	0.13932E+09	1020.1	0.1825E+05
hside_p6_top_152deg	0.18801E+09	1019.8	358.1
hside_p6_bot_156deg	0.14304E+09	1018.9	0.1123E+05
hside_p6_top_156deg	0.19015E+09	1022.6	317.0
hside_p6_bot_160deg	0.14166E+09	1021.9	0.1240E+05
hside_p6_top_160deg	0.18805E+09	1025.3	356.0
hside_p5_bot_0deg	0.14564E+08	1026.6	≥ 0.3E+5
hside_p5_top_0deg	0.18679E+08	1043.1	≥ 0.3E+5
hside_p5_bot_90deg	0.11537E+09	1007.6	≥ 0.3E+5
hside_p5_top_90deg	0.75103E+08	1009.0	≥ 0.3E+5
hside_p5_bot_180deg	0.84907E+08	1030.3	≥ 0.3E+5
hside_p5_top_180deg	0.88072E+08	1032.9	≥ 0.3E+5
hside_p5_bot_270deg	0.26565E+08	1058.4	≥ 0.3E+5
hside_p5_top_270deg	0.44141E+08	1053.8	≥ 0.3E+5
hside_p5_bot_148deg	0.15354E+09	1010.9	3640.
hside_p5_top_148deg	0.14347E+09	1014.0	8839.
hside_p5_bot_152deg	0.15970E+09	1013.9	1979.
hside_p5_top_152deg	0.14752E+09	1012.9	6107.
hside_p5_bot_156deg	0.16219E+09	1017.0	1607.
hside_p5_top_156deg	0.14988E+09	1016.1	4904.
hside_p5_bot_160deg	0.16074E+09	1016.0	1839.
hside_p5_top_160deg	0.14598E+09	1019.3	6779.
hside_p4_bot_0deg	0.34541E+08	1045.2	≥ 0.3E+5
hside_p4_top_0deg	0.50298E+08	1044.8	≥ 0.3E+5
hside_p4_bot_90deg	0.46172E+08	1021.3	≥ 0.3E+5
hside_p4_top_90deg	0.46493E+08	1025.8	≥ 0.3E+5
hside_p4_bot_180deg	0.10321E+09	1034.6	≥ 0.3E+5
hside_p4_top_180deg	0.11650E+09	1033.6	≥ 0.3E+5
hside_p4_bot_270deg	0.32764E+08	1050.6	≥ 0.3E+5
hside_p4_top_270deg	0.55100E+08	1043.3	≥ 0.3E+5
hside_p4_bot_148deg	0.16196E+09	1017.2	1630.
hside_p4_top_148deg	0.21728E+09	1017.3	136.5
hside_p4_bot_152deg	0.16378E+09	1015.9	1400.
hside_p4_top_152deg	0.21842E+09	1015.5	134.8
hside_p4_bot_156deg	0.16553E+09	1018.9	1315.
hside_p4_top_156deg	0.21621E+09	1018.3	138.1
hside_p4_bot_160deg	0.16030E+09	1021.9	1779.
hside_p4_top_160deg	0.20971E+09	1021.2	162.3
hside_p3_bot_0deg	0.39145E+08	1026.6	≥ 0.3E+5
hside_p3_top_0deg	0.59437E+08	1038.9	≥ 0.3E+5

hside_p3_bot_90deg	0.37251E+08	1023.1	≥ 0.3E+5
hside_p3_top_90deg	0.50029E+08	992.52	≥ 0.3E+5
hside_p3_bot_180deg	0.12130E+09	1030.3	≥ 0.3E+5
hside_p3_top_180deg	0.11866E+09	1027.1	≥ 0.3E+5
hside_p3_bot_270deg	0.52815E+08	1039.7	≥ 0.3E+5
hside_p3_top_270deg	0.88460E+08	1041.4	≥ 0.3E+5
hside_p3_bot_148deg	0.20319E+09	1010.9	178.6
hside_p3_top_148deg	0.18112E+09	1014.0	601.6
hside_p3_bot_152deg	0.20409E+09	1013.9	167.5
hside_p3_top_152deg	0.18201E+09	1012.9	597.8
hside_p3_bot_156deg	0.20244E+09	1012.7	174.4
hside_p3_top_156deg	0.17983E+09	1016.1	650.2
hside_p3_bot_160deg	0.19867E+09	1016.0	200.8
hside_p3_top_160deg	0.17498E+09	1019.3	848.4
hside_p2_bot_0deg	0.79729E+08	1034.1	≥ 0.3E+5
hside_p2_top_0deg	0.10882E+09	1032.0	≥ 0.3E+5
hside_p2_bot_90deg	0.74921E+08	990.75	≥ 0.3E+5
hside_p2_top_90deg	0.50642E+08	949.81	≥ 0.3E+5
hside_p2_bot_180deg	0.12332E+09	1026.2	≥ 0.3E+5
hside_p2_top_180deg	0.95666E+08	1023.8	≥ 0.3E+5
hside_p2_bot_270deg	0.14409E+09	1040.4	0.1020E+05
hside_p2_top_270deg	0.19945E+09	1039.1	199.1
hside_p2_bot_148deg	0.16468E+09	1007.5	2534.
hside_p2_top_148deg	0.15016E+09	1009.7	4117.
hside_p2_bot_152deg	0.16242E+09	1010.7	2724.
hside_p2_top_152deg	0.14807E+09	1012.7	4625.
hside_p2_bot_156deg	0.16193E+09	1014.2	2711.
hside_p2_top_156deg	0.14715E+09	1011.6	5419.
hside_p2_bot_160deg	0.15641E+09	1017.6	4178.
hside_p2_top_160deg	0.14117E+09	1015.0	9492.
hside_p1_bot_0deg	0.15127E+08	973.89	≥ 0.3E+5
hside_p1_top_0deg	0.75083E+08	986.61	≥ 0.3E+5
hside_p1_bot_90deg	0.71955E+08	970.94	≥ 0.3E+5
hside_p1_top_90deg	0.47897E+08	967.69	≥ 0.3E+5
hside_p1_bot_180deg	0.30644E+08	974.20	≥ 0.3E+5
hside_p1_top_180deg	0.83053E+08	986.74	≥ 0.3E+5
hside_p1_bot_270deg	0.59661E+08	981.66	≥ 0.3E+5
hside_p1_top_270deg	0.22322E+09	996.57	635.8
hside_p1_bot_148deg	0.90663E+08	956.41	≥ 0.3E+5
hside_p1_top_148deg	0.81363E+08	967.46	≥ 0.3E+5
hside_p1_bot_152deg	0.84828E+08	958.90	≥ 0.3E+5
hside_p1_top_152deg	0.80207E+08	970.39	≥ 0.3E+5
hside_p1_bot_156deg	0.77552E+08	961.41	≥ 0.3E+5
hside_p1_top_156deg	0.80184E+08	973.30	≥ 0.3E+5
hside_p1_bot_160deg	0.69342E+08	963.89	≥ 0.3E+5

hside_p1_top_160deg	0.79442E+08	975.91	≥ 0.3E+5
cside_p2_bot_0deg	0.15105E+08	595.89	≥ 0.3E+5
cside_p2_top_0deg	0.20620E+08	594.78	≥ 0.3E+5
cside_p2_bot_90deg	0.11479E+08	587.79	≥ 0.3E+5
cside_p2_top_90deg	0.12652E+08	586.51	≥ 0.3E+5
cside_p2_bot_180deg	0.15311E+08	595.58	≥ 0.3E+5
cside_p2_top_180deg	0.15420E+08	594.92	≥ 0.3E+5
cside_p2_bot_270deg	0.90600E+07	583.38	≥ 0.3E+5
cside_p2_top_270deg	0.64695E+07	583.54	≥ 0.3E+5
cside_p1_bot_0deg	0.34670E+07	611.69	≥ 0.3E+5
cside_p1_top_0deg	0.12020E+08	612.08	≥ 0.3E+5
cside_p1_bot_90deg	0.57174E+07	602.52	≥ 0.3E+5
cside_p1_top_90deg	0.12169E+08	602.07	≥ 0.3E+5
cside_p1_bot_180deg	0.28471E+07	607.69	≥ 0.3E+5
cside_p1_top_180deg	0.77745E+07	608.94	≥ 0.3E+5
cside_p1_bot_270deg	0.65622E+07	606.60	≥ 0.3E+5
cside_p1_top_270deg	0.26368E+08	606.62	≥ 0.3E+5